

LiqState: Liquid Identification and State Monitoring Using mmWave IoT Sensing

Fahim Niaz, Jian Zhang, Muhammad Khalid, Muhammad Younas, and Abdul Majid,

Abstract—Traditional RF-based liquid identification methods generally rely on a single characteristic such as refractive index or permittivity and often assume prior container knowledge, limiting their versatility. These approaches also face challenges in scenarios involving gradual state changes in the liquid. We propose LiqState, a contactless framework for fine-grained liquid identification and continuous state monitoring, capable of operating without prior container information. To mitigate container effects, we developed a LiqState reflection model that analyzes frequency-dependent changes, leveraging the diverse permittivity profiles of liquids across the mmWave frequency range. Our approach introduces a novel feature extraction method, VRCP, which captures four distinct physical and chemical properties for robust identification and state monitoring. Using LiqNet, a service-oriented and customized deep learning model, LiqState achieves an average classification accuracy of 97.3% across diverse conditions, accurately distinguishing 12 liquid types. Additionally, case studies highlight LiqState’s capability to monitor complex processes, such as milk fermentation (RMSE: 0.251) and fruit juice ripening (RMSE: 0.162), and differentiate between similar liquids with minimal alcohol concentration variations.

Index Terms—mmWave, Liquid Identification, Smart Sensing, Contactless Sensing, Wireless Sensing.

I. INTRODUCTION

Liquid identification is essential across industries such as security, environmental monitoring, and healthcare. Applications like liquid detection [1], security screening, water contamination detection, and blood analysis [2] benefit from accurate, non-invasive identification. Unlike humans, who rely on taste and smell, advanced systems offer precise differentiation, such as distinguishing Pepsi from Coke or detecting slight variations in alcohol content. This capability enhances product quality control and safety.

Traditional liquid identification methods rely on expensive equipment, limiting accessibility [3], [4]. Recent advancements in ubiquitous sensing technologies [5] have introduced more practical, cost-effective solutions using RFID, WiFi, and mmWave radar [6], [7]. Systems such as Tagscan [8],

Tagtag [9], WiMi [10], and FG-LiquID [11] employ innovative techniques but are primarily data-driven, limiting their ability to identify unknown liquids or monitor liquid states. LiquID [6] and Vi-Liquid [12] improve accuracy by modeling permittivity and viscosity; however, they require prior knowledge of container material and dimensions, reducing real-world applicability.

mmWave radar presents a compelling alternative due to its high-resolution sensing [13], deeper penetration through non-metallic materials, and robustness in various environments. Operating across a broad frequency range (24 GHz – 300 GHz), mmWave radar enables fine-grained differentiation based on dielectric properties and attenuation factors. Studies demonstrate its ability to achieve over 90% accuracy in liquid classification [11]. Unlike optical or RFID-based methods, mmWave radar is unaffected by ambient light and can penetrate various container materials. Compared to UWB and WiFi-based approaches, which suffer from lower frequency resolution and environmental interference, mmWave radar excels in detecting subtle state changes, such as a 1% alcohol concentration difference or gradual liquid fermentation.

Some models, including LiqDetector [14], LiqRay+ [15], and WiMi [10], address container dependence by leveraging refractive index and frequency response. However, LiqDetector depends on stable temperatures for accuracy, making it unsuitable for dynamic environments. LiqRay+ identifies liquids based on frequency response but struggles with subtle state changes. WiMi lacks the sensitivity to differentiate liquids with minor concentration variations. Furthermore, none of these methods incorporate liquid state monitoring, crucial for tracking transformations such as milk fermentation or chemical reactions in industrial processes.

These limitations highlight the need for a container-independent system capable of real-world liquid state monitoring. We introduce LiqState (Fig. 1), addressing these challenges through advanced sensing and modeling techniques. In general, the following three challenges need to be addressed:

- 1) First, fine-grained liquid identification, Differentiating similar liquids is challenging due to minimal signal variations and external interferences like multi-path effects and background noise.
- 2) Second, in the realm of fine-grained liquid detection, a major challenge lies in the system’s sensitivity to variations in temperature and frequency. Liquid properties fluctuate with environmental changes, necessitating a detection system that maintains accuracy across varying conditions and frequency bands.

Manuscript received. The paper is submitted to the IEEE Internet of Things Journal. This paper presents LiqState: Intelligent Liquid Sensing and State Monitoring via mmWave Signals Using Novel VRCP Features and Deep Learning

Fahim Niaz, Wuhan University, Wuhan China (e-mail: notify.fahim@outlook.com).

Jian Zhang is the corresponding author, Wuhan University, Wuhan China (e-mail: jzhang@whu.edu.cn).

Muhammad Khalid, University of Hull, Hull UK (e-mail: M.Khalid@hull.ac.uk).

Muhammad Younas, Wuhan University, Wuhan China (e-mail: younas@whu.edu.cn).

Abdul Majid, Wuhan University, Wuhan China (e-mail: majid20205020@gmail.com).

TABLE I: Comparison of COTS devices typically used for liquid identification with proposed LiqState

Method	Device	Container Independent	Identify Unknown Liquids	Liquid State Monitoring	Distance Independent
TagScan [8]	RFID	✓	✗	✗	✗
Tagtag [9]	RFID	✗	✗	✗	✓
FG-LiquID [11]	mmWave	✗	✗	✗	✓
LiquID [6]	UWB	✗	✓	✗	✗
WiMi [10]	WiFi	✗	✗	✗	✗
Vi-liquid [12]	UWB	✗	✓	✗	✗
LiqDetector [14]	mmWave	✓	✓	✗	✓
LiqRay [15]	USRP	✓	✓	✗	✗
LiqState	mmWave	✓	✓	✓	✓

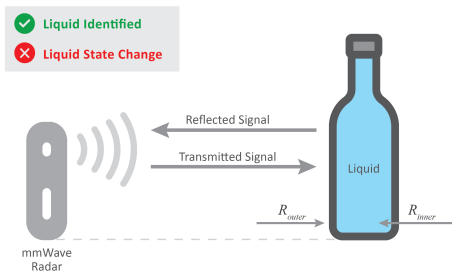


Fig. 1: An illustration of LiqState, a contactless and ubiquitous system for liquid detection and state monitoring. The system can accurately detect changes in liquid state as small as 0.1%, without the need to open the container, and operates robustly even in scenarios with random radar-target rotations and displacements.

- 3) Third, liquid state monitoring is critical in various scenarios where the physical or chemical state of a liquid can change over time due to environmental factors, processing stages, or expiration. Many liquids undergo state changes due to time, temperature, or chemical reactions. Reliable real-time monitoring is essential for ensuring product integrity and safety.

To address these challenges, we propose a ubiquitous, contactless liquid identification and state monitoring system that provides a more effective solution than existing methods, as shown in Tab. I. First, we introduce a range-FFT-based noise cancellation technique to mitigate multi-path effects and background noise, ensuring cleaner signal acquisition. Next, we present the LiqState reflection model, which eliminates the influence of container materials by leveraging the frequency-dependent nature of liquid attenuation. While containers exhibit a consistent attenuation effect across frequencies, liquids display distinct frequency-dependent attenuation characteristics. This property enables accurate, container-independent liquid differentiation.

Second, we propose VRCP, a novel feature extraction model for fine-grained liquid detection. VRCP identifies key physical and chemical properties, such as viscosity, refractive index, permittivity, and phase shifts, independent of temperature and frequency. These intrinsic properties remain stable regardless

of environmental factors, enabling accurate detection across diverse conditions.

Third, we leverage the mmWave phase component, which is highly sensitive to minor liquid composition changes. Our observations show that liquid undergoing physical or chemical transformations induces a 180-degree phase shift in mmWave signals. By extracting these phase-related features, our system continuously tracks liquid state changes, offering real-time updates without invasive methods.

In summary, The major contributions of LiqState are:

We introduce LiqState, a ubiquitous and contactless system capable of precisely distinguishing and monitoring liquid states, even in scenarios with extremely subtle content variations, such as a 0.1% v/v difference. LiqState maintains its accuracy and robustness under various radar target displacements and rotations, demonstrating its flexibility and practicality in real-world applications. We build a LiqState reflection model, which eliminates the influence of the container material. By using the fact that the attenuation factor of the container remains constant across frequencies, while the attenuation of liquids changes with frequency, we designed a relative frequency response factor. This factor represents the relative difference in attenuation across multiple frequencies, allowing LiqState to identify liquids and monitor their states independently of the container material. We propose VRCP, a novel feature extraction model that captures inherent liquid properties such as viscosity, refractive index, complex permittivity, and phase shifts, without being affected by temperature or frequency variations. Prior studies have demonstrated the effectiveness of individual features like complex permittivity [16], viscosity [17], and refractive index [14] for liquid identification. However, relying on a single feature limits versatility in diverse scenarios. VRCP overcomes this by combining all four features, providing complementary, non-redundant information essential for fine-grained liquid identification and state monitoring. This model is supported by mathematical proof based on physics concepts, ensuring the accurate extraction of these four primary features for fine-grained liquid identification and state monitoring. To validate our approach, we implemented a customized deep

neural network prototype, LiqNet. This prototype can be deployed as a service-oriented solution, compatible with smartphones and laptops, making it versatile for both mobile and desktop applications. We conducted extensive experiments across multiple use cases, including detecting alcohol concentration, oil purity, milk fat content, and coffee strength. Several case studies further demonstrate the system's accuracy and robustness in various real-world scenarios, showcasing its potential as a practical solution for industries requiring precise liquid monitoring and identification.

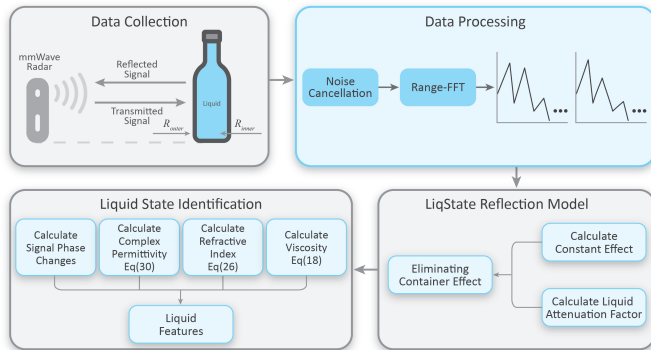


Fig. 2: Workflow of the LiqState System. The sensed signals undergo preprocessing to remove noise and mitigate multipath effects. Next, Range-FFT is applied, and signals are cropped to highlight the target zone, capturing discriminative fine-grained information. The LiqState reflection model is then used to remove container effects. Finally, four key features are extracted, enabling accurate liquid identification and state monitoring.

II. RELATED WORK

Recent advancements in sensor-based material identification have led to a surge in innovative techniques across various domains, particularly for identifying liquids, which remains both promising and challenging. Traditional methods for identifying liquids typically rely on specialized, high-cost equipment to analyze material properties [18], [19], [20]. These approaches leverage the fundamental principle that different substances exhibit distinct absorption and reflection characteristics when exposed to light waves. However, they often necessitate direct contact with the liquid, such as immersing a probe to capture signals, followed by spectral analysis using a spectrometer. While effective, these techniques are impractical for widespread, everyday applications such as identifying liquids within sealed containers due to their complexity, cost, and lack of non-invasive capabilities. Liquid detection research can broadly be categorized into three approaches: Radio Frequency (RF)-based, optical and camera-based, and mmWave-based material identification.

A. RF-Based Material Identification

RF technology has gained significant attention in liquid identification, producing two primary approaches: data-driven and model-driven methods.

- **Data-Driven Methods:** These approaches typically require pre-trained datasets to classify liquids. TagScan [8] uses RFID readings, extracting RSSI and phase data to create a database of 10 liquids. Tagtag [9] attaches RFID tags directly to targets, detecting adulterants like fake alcohol and expired milk by comparing the data to pre-trained samples. FG-LiquID [11] takes this further by using mmWave radar and neural networks to identify 30 liquids. However, this method struggles with unknown liquids and requires extensive database creation.
- **Model-Driven Methods:** These techniques aim to calculate the physical properties of liquids, like permittivity. LiquID [6], for instance, computes the complex permittivity by analyzing signal amplitude and phase, enabling the identification of 33 liquids. Vi-Liquid [12] measures liquid viscosity through mechanical waves, recognizing up to 30 different types. While these models are effective, they often depend on prior knowledge about the container's material and dimensions, which limits versatility. To address this, we developed a container-independent system by incorporating dual-antenna technology and analyzing the relative frequency response.

B. Optical and Camera-Based Systems

Optical systems use thermal infrared sensors, photodiodes, and visible light cameras to analyze liquid properties through optical absorption or reflection. This method effectively reveals characteristics by studying spectral signatures. For example, Nutrilizer [21] employs photoacoustic sensing, using light modulation to generate liquid-specific spectra that identify nutrients and adulterants. Smart-U [22] uses LEDs and photodiodes to recognize liquids on a spoon by measuring how various substances affect absorption. AI-light [23] introduces a smart ice cube that estimates alcohol concentration via near-infrared spectrometry. Although these systems provide high accuracy, they require specialized devices, limiting accessibility to everyday users. To bridge this gap, Vi-Liquid offers a smartphone-compatible solution, making liquid testing more accessible and practical.

C. mmWave-Based Sensing

The rapid evolution of 5G technology has highlighted mmWave radio signals as a powerful tool for liquid identification. mmWave's short wavelength and high directionality make it ideal for fine-grained sensing applications. This includes tasks like environment mapping [24], [24], human tracking [25], [26], counterfeit currency [27], [28] and even vital sign monitoring [29], [30]. In liquid identification, mmWave's precision makes it particularly effective. It has been employed in various fields, such as gesture recognition [31]. By leveraging this technology, mmWave offers unique advantages for liquid detection, enabling precise identification and phase shift monitoring, even in challenging environments.

Our study utilized the LiqState system, which monitors the phase shifts of liquids during state transitions. For example, during the fermentation of milk to yogurt, LiqState effectively

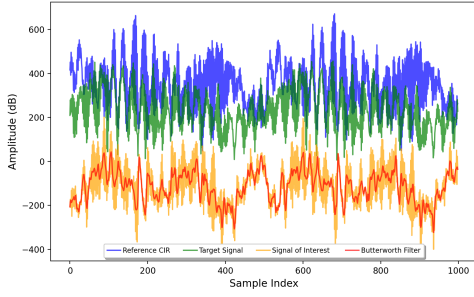


Fig. 3: Elimination of multi-path effects using Reference Channel Impulse Response (CIR) and noise reduction through Butterworth high-pass filtering.

tracked phase changes as a function of time and chemical reactions, providing valuable insights into the liquid's changing properties. Such applications highlight the utility of mmWave sensing in both industrial and consumer-grade liquid testing systems.

III. SYSTEM OVERVIEW

The LiqState, illustrated in Fig. 2, comprises four key modules. The first module handles data collection using a COTS mmWave radar mounted on a tabletop platform. This setup enables the radar to transmit and receive signals at multiple angles, maximizing data coverage. The raw data collected by the radar is initially processed through filtering and pre-processing techniques to suppress noise, mitigate hardware-induced disturbances, and remove ambient interference from the intermediate frequency (IF) signal. The second module involves the construction of the LiqState reflection model, designed to eliminate the container's effect. This model compensates for the constant impact of the container across different frequencies and adjusts for the frequency-dependent attenuation properties of the liquid being analyzed. Finally, The system performs fine-grained liquid detection by extracting four critical liquid properties such as viscosity, refractive index, complex permittivity, and phase shift of the signal. These properties are used to derive relative features that remain stable, independent of environmental factors such as temperature and frequency fluctuations.

A. Noise Cancellation

In signal preprocessing, the multi-path effect introduces various signal components beyond the direct reflection from the target (e.g., a liquid container). These components include Direct Current (DC) offsets, ambient noise, and reflections from other surfaces. To address these issues, we utilize a Channel Impulse Response (CIR) to capture and isolate the multi-path effects and background noise.

The CIR under the influence of multi-path can be defined as:

$$g(\lambda) = \sum_{i=1}^N b_i e^{-j\phi_i \lambda} \delta(\lambda - \lambda_i) \quad (1)$$

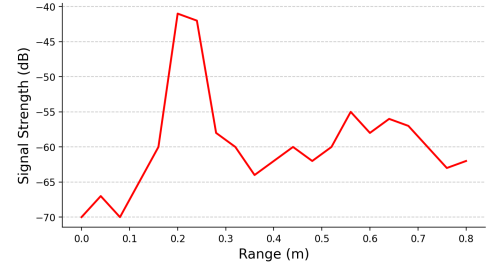


Fig. 4: Target zone peak detection using Range-FFT

where: N is the total number of signal paths, b_i , ϕ_i , and λ_i represent the amplitude, phase, and time delay of the i -th path, $\delta(\lambda)$ is the Dirac delta function representing the impulse response. To mitigate noise, we adopt a reference CIR $g_r(\lambda)$, captured when there is no liquid present in front of the radar. This reference CIR suppresses the DC component, ambient reflections, and background noise. Since the detection environment remains stable, the reference CIR can be reused without repeated sampling. The CIR is calculated by averaging multiple samples to suppress unstable noise components:

$$g_r(\lambda) = \frac{1}{M} \sum_{k=1}^M g(\lambda, t_k) \quad (2)$$

where: M is the total number of sampling instances. To isolate the signal reflected by the target (i.e., the liquid), we subtract the reference CIR from the measured CIR at time t :

$$g_t(\lambda) = g(\lambda, t) - g_r(\lambda) \quad (3)$$

Here, $g_t(\lambda)$ represents the signal of interest, free from multipath distortions and background noise. After eliminating the multipath effect through the reference CIR, we apply a Butterworth filter to further suppress high-frequency noise and refine the signal as shown in Fig. 3. The Butterworth filter is characterized by a flat frequency response in the passband, ensuring minimal signal distortion. The transfer function of an m -th order Butterworth filter [32] is given by:

$$F(\nu) = \frac{1}{\sqrt{1 + \left(\frac{\nu}{\nu_c}\right)^{2m}}} \quad (4)$$

where: ν is the frequency of the signal, ν_c is the cutoff frequency, and m is the filter order. The filtered output $g_{\text{filtered}}(t)$ is obtained by applying the Butterworth filter to the signal $g_t(\lambda)$:

$$g_{\text{filtered}}(t) = F(\nu) \cdot g_t(\lambda) \quad (5)$$

Finally, as shown in Fig. 4 the noise-free signal can be expressed as:

$$g_{\text{output}}(t) = F(\nu) \cdot (g(\lambda, t) - g_r(\lambda)) \quad (6)$$

B. Range-FFT

In liquid identification using mmWave radar, the range-FFT plays a crucial role in analyzing reflected radar signals to determine the distance to various reflective surfaces within the

liquid and its container. The transmitted FMCW chirp signal [33] interacts with the liquid, and the received signal carries information about the liquid's dielectric properties, such as permittivity and attenuation, which impact signal propagation. The beat frequency f_b , corresponding to the distance R of the reflection surface, is calculated using the formula:

$$f_b = \frac{2BR}{cT_{\text{chirp}}} \quad (7)$$

Where $B = 4 \text{ GHz}$ is the chirp bandwidth, $T_{\text{chirp}} = 40 \mu\text{s}$ is the chirp duration, c is the speed of light, and R represents the distance to the reflection surface. By applying the range-FFT to the received signal, we transform the time-domain signal into the frequency domain, as illustrated in Fig. 4. In this transformed spectrum, peaks indicate reflections from different interfaces, such as the liquid surface or container walls. The distance R for each peak is then determined by:

$$R = \frac{cT_{\text{chirp}}f_b}{2B} \quad (8)$$

The dielectric properties of the liquid influence the propagation speed of the radar signal, with higher permittivity slowing the signal and resulting in detectable shifts in the beat frequency.

C. LiqState Reflection Model

Liquid identification using mmWave is complicated by signal reflections from containers, which can distort measurements. The LiqState reflection model overcomes this by integrating reflection-based and frequency-dependent attenuation models, ensuring accurate liquid characterization. We first analyze radar reflections when targeting a liquid-filled container. Then, the LiqState model isolates the liquid's reflection by calculating the container's constant effect and the relative frequency of reflected signals. This works on two principles: (1) container reflections remain nearly constant across frequencies, while (2) liquid attenuation varies with frequency due to molecular interactions, allowing precise liquid identification.

1) *The Constant Nature of Container Reflections Across Frequencies:* The radar signal experiences multiple reflections when interacting with the container. As shown in Fig. 1, these reflections include the surface reflection at the container's outer surface R_{outer} and the liquid surface reflection at the liquid-container interface R_{inner} . For most non-metallic containers, the refractive index remains nearly constant across the different frequencies (for example, the refractive index of glass is about 1.5, while the refractive index of water is close to 9). As a result, the container introduces a constant reflection across frequencies, which can be modeled and separated from the liquid's signal by leveraging the stability of the container's response. The signal reflection coefficients at the outer and inner interfaces can be expressed using Fresnel's equations as:

$$R_{\text{outer}} = \left(\frac{n_{\text{air}} - n_{\text{Conti}}}{n_{\text{air}} + n_{\text{Conti}}} \right)^2 \quad (9)$$

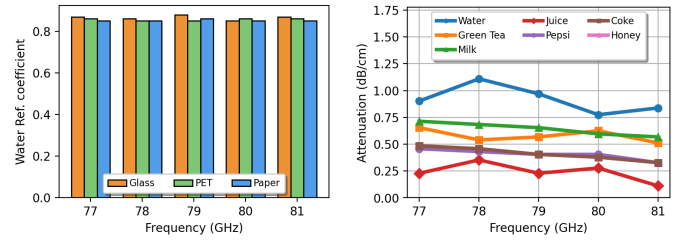
$$R_{\text{inner}} = \left(\frac{n_{\text{Conti}} - n_{\text{Liq}}}{n_{\text{Conti}} + n_{\text{Liq}}} \right)^2 \quad (10)$$

Where n_{air} is the refractive index of air (approximately 1), n_{Conti} is the refractive index of the container (constant across frequencies), and n_{Liq} is the refractive index of the liquid (frequency-dependent). These coefficients represent the ratio of reflected to incident wave energy at each interface.

To present the effect of the liquid and the container on the reflected signal, we express the amplitude of all the reflected signals. First, we take the external air and the container as a mixing medium. According to the Friis transmission equation [34], the amplitudes of signals reflected from R_{outer} and R_{inner} can be expressed as:

$$S_{\text{outer,inner}} = P_t R_t R_r \frac{\lambda}{4\pi L} (R_{\text{outer}} + R_{\text{inner}} e^{-2\alpha d}) \quad (11)$$

Where P_t is the amplitude of the transmitted radar signal, $R_t R_r$ are the antenna gains for transmission and reflection, λ is the wavelength of the radar signal, L is the distance from the radar to the target surface, α is the attenuation factor for the liquid, and d is the thickness of the container.



(a) Container effect remains constant (b) Attenuation factors vary across liquids for the same liquid type.

Fig. 5: The container effect remains the same for the same type of liquid, while the attenuation factors of various liquids change for frequency.

2) The Frequency-Dependent Attenuation of the Liquid:

The impact of the container on the signal amplitude mainly comes from two aspects: the refraction of the medium and the transmission distance of the signal in the liquid, both of which are related to the refractive index. As a result, the effect of the container on the signal amplitude is almost invariant with frequency. This allows us to use ratios of different frequency signals to remove its effect. In Fig. 5, when the signal frequency is changed, the effect of the container remains stable and at the same time, the attenuation factor of different liquids has different trends [35]. The liquid's attenuation factor $\alpha(f)$ varies significantly with frequency. This variation arises due to the molecular polarization and interactions of the liquid with the radar signal. By leveraging this frequency dependency, we can isolate the liquid's unique signal response from that of the container. The attenuation factor $\alpha(f)$ describes the exponential decay of the radar signal as it passes through the liquid. The relationship between the attenuation and the signal can be expressed as:

$$S_{\text{att}}(f) = S_0 e^{-\alpha(f)d} \quad (12)$$

Where $S_{\text{att}}(f)$ is the attenuated signal at frequency f , S_0 is the initial signal before attenuation, and $\alpha(f)$ is the attenuation coefficient of the liquid, which depends on frequency. To eliminate the constant container reflection and isolate the frequency-dependent liquid response, we use a relative frequency response. This is the ratio of signals at two different frequencies, f_1 and f_2 , expressed as:

$$R_{f_1, f_2} = \frac{S_{\text{att}}(f_1)}{S_{\text{att}}(f_2)} = e^{(\alpha(f_2) - \alpha(f_1))d} \quad (13)$$

The Eq. 13 allows us to compare how the signal changes with frequency, eliminating the container's constant contribution, and providing a feature that is dependent on the liquid's attenuation properties. So, both the constant nature of the container reflections and the frequency-dependent attenuation of the liquid are expressed as:

$$R_{\text{Liq}} = \frac{S_{\text{att}}(f_1)}{S_{\text{att}}(f_2)} = \frac{R_{\text{outer}} + R_{\text{inner}}e^{-2\alpha(f_1)d}}{R_{\text{outer}} + R_{\text{inner}}e^{-2\alpha(f_2)d}} \quad (14)$$

To sum up, with the proposed LiqState-reflection model, we can obtain the liquid's properties without needing to know the container's material effect. As a result, container-independent liquid detection is achieved.

IV. VRCP: FINE-GRAINED LIQUID IDENTIFICATION

In liquid identification, selecting physical and chemical properties is essential for distinguishing liquid types, especially for fine-grained categorization. This paper introduces VRCP: viscosity, refractive index, complex permittivity, and phase shift due to state changes. As shown in Tab. II, these parameters offer distinct insights into liquid behavior, enabling a robust feature set for accurate identification of unknown liquids. VRCP achieves identification independent of temperature and frequency fluctuations. The refractive index, for example, can vary with external temperature [14], while complex permittivity shifts across frequencies [15]. To mitigate these factors, VRCP combines refractive index, viscosity, complex permittivity, and phase shift into a unified feature set. Leveraging the stability of some properties and the complementary nature of their variations, VRCP reduces temperature and frequency impacts on individual measurements. This approach provides a consistent and accurate method for fine-grained liquid and state identification across diverse environmental conditions.

A. Detection of Liquid by Calculating the Liquid Viscosity

Viscosity is a fundamental property of liquids that measures their internal resistance to flow. It arises due to the interactions between liquid molecules and is influenced by temperature, pressure, and molecular composition. When mmWave radar waves interact with a liquid, the liquid's viscosity can influence the attenuation and phase shift of the signal, which can be measured and used to estimate the viscosity.

Viscosity, denoted by η , is a measure of a fluid's resistance to deformation or flow. In the context of radar-based liquid detection, the viscosity is related to the interaction between the liquid and the propagating radar waves. To develop a

model, we need to account for both the mechanical properties of the liquid (viscosity) and the way the electromagnetic waves propagate through the liquid medium. When radar waves propagate through a viscous liquid, the wave experiences attenuation (energy loss) and phase shift. These changes can be linked to the liquid's viscosity. The electric field E of the radar wave passing through a liquid with viscosity η can be described by the wave equation:

$$\nabla^2 E - \frac{1}{c^2} \frac{\partial^2 E}{\partial t^2} = 0 \quad (15)$$

However, when a liquid is viscous, energy dissipation occurs [36], leading to an additional term related to the viscosity of the medium. This can be expressed as:

$$\nabla^2 E - \frac{1}{c^2} \frac{\partial^2 E}{\partial t^2} = \mu\eta \frac{\partial E}{\partial t} \quad (16)$$

where: c is the speed of light in the medium, μ is the magnetic permeability of the liquid, η is the dynamic viscosity of the liquid, and the term $\mu\eta \frac{\partial E}{\partial t}$ represents the viscous dissipation of energy in the liquid. The attenuation of the wave as it passes through the liquid is proportional to the viscosity. The signal's amplitude $A(t)$ decays exponentially as it propagates through the liquid, and the decay can be modeled as:

$$A(x) = A_0 e^{-\alpha x} \quad (17)$$

where: A_0 is the initial amplitude, α is the attenuation coefficient, and x is the distance traveled by the wave through the liquid. The attenuation coefficient α is related to the viscosity [35] of the liquid by:

$$\alpha = \frac{\eta\omega^2}{2\rho c^3} \quad (18)$$

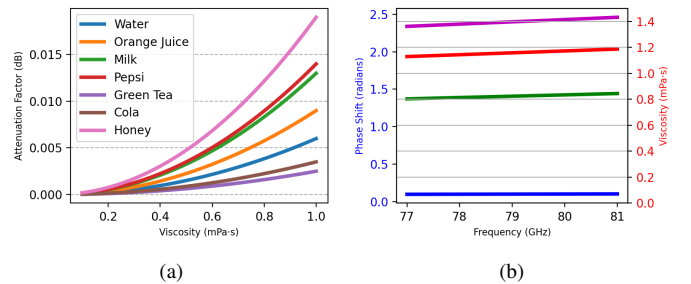


Fig. 6: Comparison of viscosity's effects on attenuation and phase shifts.

Eq. 18 shows that as the viscosity η increases, the attenuation of the signal also increases as illustrated in Fig.6a Where ω is the angular frequency of the radar signal, ρ is the density of the liquid, and c is the speed of the electromagnetic wave in the liquid. Furthermore, the radar signal also experiences a phase shift $\Delta\phi$ as it passes through the viscous liquid. The phase shift is directly related to the liquid's viscosity and the distance traveled by the wave. The phase shift can be modeled as:

$$\Delta\phi = \frac{\omega d}{c} - \frac{\eta d}{2c^2} \quad (19)$$

The phase shift provides an indirect measure of the liquid's viscosity [37], as shown in Fig.6b, higher viscosity leads to

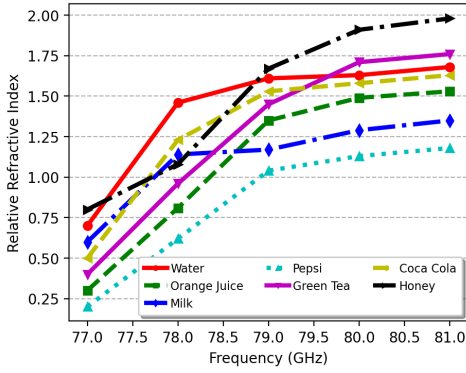


Fig. 7: Relative refractive index of various liquids across different frequencies

larger phase shifts for the same signal frequency and liquid thickness. We combine the attenuation and phase shift effects to estimate the viscosity η of the liquid. By measuring both the amplitude decay and phase shift of the radar signal, we can solve for the viscosity using the following relations:

$$\eta = \frac{2\rho c^3 \alpha}{\omega^2}, \quad \eta = \frac{2c^2 \Delta\phi}{d} \quad (20)$$

Eventually, Eq. 20 gives the viscosity of a liquid based on the radar signal's amplitude attenuation and phase shift. By combining the attenuation and phase shift information, we can accurately estimate the viscosity of the liquid, independent of other factors such as temperature or frequency.

B. Liquid Detection Using Refractive Index

Accurate liquid detection and refractive index measurement are critical in fields like material characterization, quality control, and environmental sensing. Using mmWave, we can non-invasively measure these properties by analyzing transmission and reflection at the air-liquid interface. This method can also eliminate the effects of the container and focuses on the physical properties governed by the Fresnel equations.

The Fresnel equations describe how electromagnetic waves interact at the boundary between two different media, such as air and liquid [38]. At normal incidence ($\theta_i = 0$), the reflection and transmission coefficients are given by:

$$R_{Liq} = \left(\frac{n_{air} - n_{Liq}}{n_{air} + n_{Liq}} \right)^2 \quad (21)$$

The transmission coefficient at normal incidence is:

$$T_{Liq} = \frac{4n_{air}n_{Liq}}{(n_{air} + n_{Liq})^2} \quad (22)$$

Where: $n_{air} \approx 1$ is the refractive index of air and n_{Liq} is the refractive index of the liquid.

For oblique incidence at an angle θ_i , we must account for the polarization of the wave (s-polarized or p-polarized). For s-polarized waves (electric field perpendicular to the plane of incidence), the reflection coefficient is:

$$R_s = \left(\frac{n_{air} \cos \theta_i - n_{Liq} \cos \theta_t}{n_{air} \cos \theta_i + n_{Liq} \cos \theta_t} \right)^2 \quad (23)$$

Similarly, for p-polarized waves (electric field parallel to the plane of incidence), the reflection coefficient is:

$$R_p = \left(\frac{n_{Liq} \cos \theta_i - n_{air} \cos \theta_t}{n_{Liq} \cos \theta_i + n_{air} \cos \theta_t} \right)^2 \quad (24)$$

Here, θ_t is the transmission angle, related to the incidence angle θ_i by Snell's Law:

$$n_{air} \sin \theta_i = n_{Liq} \sin \theta_t \quad (25)$$

The transmission coefficients for s-polarized and p-polarized waves are given by:

$$T_s = \frac{2n_{air} \cos \theta_i}{n_{air} \cos \theta_i + n_{Liq} \cos \theta_t} \quad (26)$$

$$T_p = \frac{2n_{air} \cos \theta_i}{n_{Liq} \cos \theta_i + n_{air} \cos \theta_t} \quad (27)$$

Solving the Fresnel equation for the refractive index at normal incidence gives:

$$n_{Liq} = 1 + \sqrt{R_{Liq}} / (1 - \sqrt{R_{Liq}}) \quad (28)$$

For oblique incidence, the refractive index can be calculated using the measured reflection and transmission coefficients (R_s , R_p , T_s , and T_p), along with Snell's Law.

Fig. 7 demonstrates the relative variation of the transmission coefficient with frequency for seven common liquids, which is calculated using Eq. 28. This analysis is essential for understanding how small fluctuations in frequency impact the refractive index and, consequently, the transmission properties of these liquids.

C. Detection of Liquid by Calculating the Complex Permittivity

When mmWave radar signals interact with a liquid, the real part represents energy storage, while the imaginary part reflects conductivity and energy loss as heat. Both vary with frequency and composition, making complex permittivity essential for fine-grained liquid identification. The material's electromagnetic response is governed by Maxwell's equations. Maxwell's 4th equation is particularly relevant here as it describes how the magnetic field (h) interacts with electric currents (j) and the rate of change of electric displacement ($\frac{\partial d}{\partial t}$):

$$\nabla \times h = j + \frac{\partial d}{\partial t} \quad (29)$$

Where h is known as magnetic induction whose value is:

$$h = \frac{1}{\mu_0} (b - m) \quad (30)$$

Where b is the magnetic field and m is magnetization, j is the current density and d is electric displacement, which is given as:

$$d = \epsilon \gamma \quad (31)$$

Here ϵ is the permittivity of the material and γ is the electric field. The above equation can be written as:

$$\nabla \times h = (\sigma \gamma + b f \epsilon) \gamma \quad (32)$$

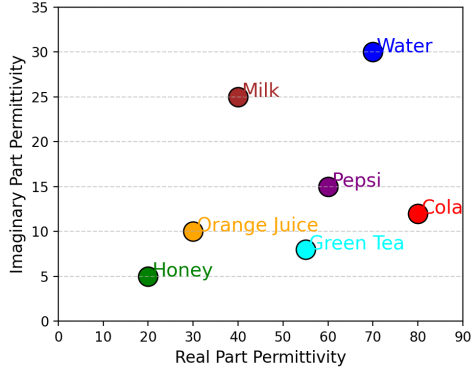


Fig. 8: The real and imaginary parts of the mmWave signal enable the identification of different liquids

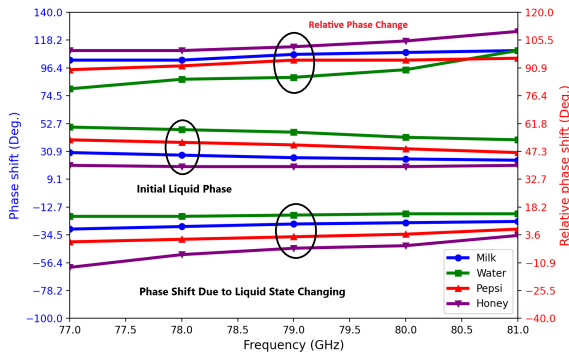


Fig. 9: Phase change due to the variation in liquid state

Here ϵ' is the phasor operator, $b^2 = -1$. At low frequencies, the electric field easily aligns with dipole rotations, resulting in a high ϵ' (real part of permittivity) and a low ϵ'' (imaginary part, or loss factor). As the frequency increases, the dipoles rotate faster, causing an increase in ϵ'' , indicating higher energy loss. However, the dipoles can no longer keep up with the rapidly oscillating electric field at very high frequencies, decreasing both ϵ' and ϵ'' . According to the theoretical model, the imaginary part of the complex permittivity, ϵ'' , is expected to increase initially with frequency and then decrease at higher frequencies. As shown in Fig.8, the experimental results align with the theoretical expectations, though the rate of change varies for each liquid.

TABLE II: Comparison of selected liquids based on their physical and electromagnetic properties

Liquid	Viscosity (mPa.s)	Ref. Index (77-81GHz)	Phase Shift	ϵ'	ϵ''
Water	0.980	8.5–9.0	35°–50°	78.5–81.0	0.5–1.0
Milk	1.5–3.4	4.0–6.0	25°–40°	3.5–4.0	0.15–0.25
Fruit Juice	55–75	3.5–5.5	20°–35°	4.0–5.0	0.2–0.4
Green Tea	1.0–1.2	4.0–5.0	15°–25°	3.5–4.5	0.1–0.3
Coca Cola	1.6–1.8	3.5–4.5	30°–45°	3.0–4.0	0.2–0.4
Cooking Oil	1400	1.5–2.0	10°–20°	2.5–3.0	0.05–0.15
Coffee	75–85	3.0–5.0	25°–35°	4.0–5.0	0.15–0.35
Honey	150–225	6.0–8.0	35°–50°	5.0–6.0	0.25–0.5
Fanta	1.5–1.8	3.5–4.5	30°–45°	3.0–4.0	0.2–0.3
Vinegar	1.8–2.0	4.0–5.0	30°–40°	4.0–5.0	0.15–0.25
Sprite	1.0–1.2	3.5–4.5	30°–45°	3.0–4.0	0.15–0.25

D. Detection of Liquid State Using Signal Phase Shift

Detecting liquid state changes, such as freezing, evaporation, or spoilage, using mmWave involves analyzing the phase shift of reflected electromagnetic waves. The method relies on observing how the radar signal, operating in the frequency range of 77-81 GHz, interacts with the liquid's surface. Variations in density, dielectric properties, and molecular structure during state changes alter the propagation of these waves, making it possible to identify the transition.

When a liquid undergoes a state change, its relative permittivity (ϵ_r), which is a measure of how it interacts with electromagnetic fields, varies. This change in permittivity affects the phase of the reflected mmWave signal, providing insights into the liquid's state. The wavelength λ of a mmWave radar signal propagating through a liquid is defined by the equation:

$$\lambda_{\text{liq}} = \frac{c}{f\sqrt{\epsilon_r}} \quad (33)$$

Where: c is the speed of light in a vacuum, f is the frequency of the radar wave, and ϵ_r is the relative permittivity of the liquid. The phase of the mmWave radar signal is related to the distance traveled, x , by:

$$\phi = \frac{2\pi x}{\lambda} \quad (34)$$

The phase shift, $\Delta\phi$, due to the liquid's thickness d is given by:

$$\Delta\phi = \frac{4\pi f d \sqrt{\epsilon_r}}{c} \quad (35)$$

By continuously measuring $\Delta\phi$, we can monitor changes in the liquid's state. For instance, the phase shift varies when a liquid transitions from one state to another (e.g., from liquid to solid) because changes in density and molecular structure directly influence ϵ_r . The sensitivity of the phase shift to changes in permittivity is described by the derivative:

$$\frac{\partial\phi}{\partial\epsilon_r} = \frac{4\pi f d}{c\sqrt{\epsilon_r}} \quad (36)$$

Eq. 36 demonstrates that phase shift measurements can detect subtle changes in a liquid's dielectric properties, making it effective for identifying state changes. Fig. 9 illustrates the phase and relative phase shifts observed in four liquids (milk, water, Pepsi, and honey) using mmWave across different frequency range. Initially, the phase shift was calculated for each liquid in its stable state. Subsequently, 10% and 20% sucrose solutions were added to each liquid, resulting in detectable phase shifts. The observed phase shifts due to the liquid state changes indicate significant alterations when adding sucrose, highlighting changes in the liquid's molecular composition and viscosity. These results demonstrate that mmWave radar is highly sensitive to variations in liquid states, with measurable changes corresponding to their molecular structure and viscosity. When electromagnetic waves reflect from a liquid surface, the amplitude of the reflected wave, W_R , is related to the amplitude of the incident wave, W_I , by:

$$W_R = \left(\frac{\eta_1 - \eta_2}{\eta_1 + \eta_2} \right) W_I \quad (37)$$

Where: η_1 and η_2 are the impedance of the incident and transmitted medium, respectively. For waves reflecting from a denser medium, the reflected wave undergoes a phase inversion of 180°:

$$W_R = \left(\frac{v_1 - v_2}{v_1 + v_2} \right) W_I \quad (38)$$

Analyzing the phase and amplitude of the reflected waves makes it possible to monitor state changes in real time. This method has wide-ranging applications in industries where the precise detection of liquid states is critical, such as in food processing, chemical manufacturing, or environmental monitoring.

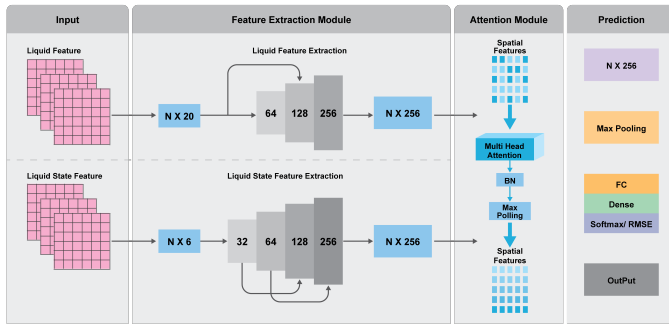


Fig. 10: LiqNet model architecture for liquid identification.

V. LIQNET OVERVIEW

Our approach for fine-grained liquid identification and state monitoring using LiqNet tackles two main challenges: (i) Extracting detailed, discriminative features for precise liquid identification, and (ii) Tracking state changes through mmWave phase signal analysis. We introduce LiqNet (Fig. 10), a neural network architecture designed to automatically capture these features and monitor liquid states in real time. LiqNet’s residual layer architecture with linear transformations enables it to detect subtle changes in liquid properties and transitions, making it ideal for fine-grained identification tasks. The network integrates two core components: (i) a feature extraction module, and (ii) an attention module based on spatial features. The feature extraction module, using residual layers, generates both local and global features to capture variations across different liquid compositions.

A. LiqNet Input

As shown in Fig. 10, LiqNet consists of four key components: (i) liquid feature extraction, (ii) liquid state feature extraction, (iii) attention module, and (iv) prediction layer. The input data is divided into two categories: liquid features and liquid state features. Liquid features include essential properties like viscosity, refractive index, and complex permittivity, while liquid state features are represented by signal phase shifts to capture state transition information. The liquid

features are fed into the liquid feature extraction module, where the input dimensions are $N \times 3$ (liquid properties) $\times 5$ (frequencies) +3 additional absolute features. These are flattened to dimensions of $N \times 18$ before being processed by a 3-layer residual CNN. This module utilizes residual connections to retain critical low-level features, allowing deeper layers to extract more complex patterns.

Similarly, the liquid state features, composed of phase shift data with dimensions $N \times 1$ (phase feature) $\times 5$ (frequencies) +1 absolute feature, are input into the liquid state feature extraction module. This module, using a 4-layer residual CNN, captures both local and global signal characteristics. The residual CNN structure efficiently handles phase shift variations, ensuring that subtle shifts due to liquid state transitions are identified. After feature extraction, the data passes through a multi-head attention module, which enhances LiqNet’s focus on the most informative features. Using max-pooling across feature vectors, the attention module calculates attention weights for each channel. These weights are adaptively learned through non-linear transformations, incorporating normalization, dropout, and activation functions. Finally, LiqNet outputs the specific liquid category and determines if its state has changed.

TABLE III: Runtime Complexity and Analysis of LiqNet

Processing Stage	Complexity	Runtime Analysis (ms)
Feature Extraction	$O(N * k * f)$	12.3
Attention Mechanism	$O(N^2)$	18.6
Prediction Layer	$O(N * d)$	8.5
Total Complexity	Dominated by $O(N^2)$	39.4

VI. EVALUATION

Implementation setup: To implement LiqState, we utilize the IWR1443 mmWave radar [39] (77-81 GHz) with the DCA1000EVM for data acquisition. The radar includes two transmitting and four receiving antennas, delivering a peak gain of 7 dBi and providing a 120° horizontal field of view (FoV). The IWR1443ISK’s antenna has dimensions of 8 mm, which corresponds to a radiated far-field boundary of approximately 3 cm. It uses an open setup without additional radome enclosures to minimize signal attenuation and reflection artifacts also it operates within the FCC/ETSI regulatory limits for short-range radar applications. We configured the system with a frequency slope of 65.000 MHz/ μ s and a sample rate of 4000 ksp/s, generating 128 chirps per frame and 256 ADC samples per chirp. This setup results in a range resolution of 3.55 cm and a velocity resolution of 11.77 cm/s. Notably, LiqState requires only one pair of transmitting and receiving antennas for effective liquid detection and state monitoring.

Environment setup: As shown in Fig. 11, the mmWave radar was positioned 0.2 m away from the liquid containers. Data collection was conducted by transmitting mmWave signals at five different frequencies. A container filled with liquid was placed in front of the radar to ensure consistent measurement conditions.

Liquids and containers: As illustrated in Fig. 12, we evaluated the performance of LiqState using twelve types of liquids

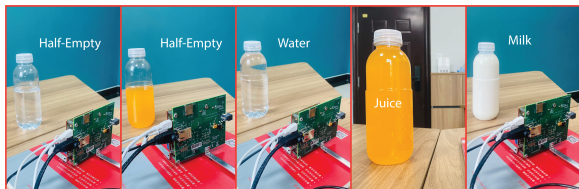


Fig. 11: Experimental Setup

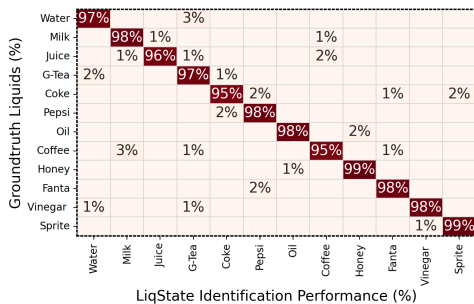


Fig. 12: Overall performance of LiqState in identifying 12 types of liquids

and three different containers. The liquids tested include water, milk, juice, green tea, Pepsi, Coca-Cola, oil, coffee, honey, Fanta, Vinegar, and Sprite. For containers, we selected three common materials: PET (Polyethylene-Terephthalate), HDPE (High-Density Polyethylene), and glass. Additionally, to assess the impact of container dimensions, PET containers were tested in three different calibers: 5.5 cm, 7 cm, and 7.5 cm.

Data Collection: To build a comprehensive benchmark and evaluate LiqState’s fine-grained liquid and state identification performance, we selected a diverse range of liquids from a local supermarket. For each liquid, we conducted three independent data collection sessions over a week. In each session, 250 ml of liquid was poured into a container placed 20 cm from the radar. The positioning was repeated 10 times per session, with slight, randomized displacements and orientation changes ranging from -4 cm to +4 cm in displacement and 0° to 180° in orientation. After each adjustment, the mmWave radar was activated for 10 seconds to stabilize before recording signals. All liquids were kept at a room temperature of 30°C. We collected 20 samples per liquid across five different frequencies and 10 different positions, resulting in 1,000 samples per liquid. For 12 different types of liquids, we obtained 12,000 training samples and gathered 3,000 samples for the test dataset.

VII. OVERALL PERFORMANCE

To evaluate the overall performance of LiqState, we conducted two types of assessments. First, we tested LiqState’s ability to identify different types of liquids accurately. Second, we evaluated its performance in detecting both minor and major changes in the state of the liquid, ensuring its robustness in identifying subtle and significant state transitions.

We first ranked the liquid categories based on their average absolute feature values. Then, we assessed LiqState’s performance using a 5-fold cross-validation method. As depicted

TABLE IV: LiqState Performance Evaluation in Liquid State Monitoring

Liquid State Change	RMSE
Milk to Yogurt	0.294
Adding Sugar in Water	0.265
Adding Water in Honey	0.271
Adding Sugar in Pepsi	0.201
Adding Sugar in Green Tea	0.283
Overall RMSE	0.292

in Fig. 12, the confusion matrix illustrates the identification results for the 12 liquid categories tested. LiqState achieved an average accuracy of 97.3% across the different fluid types. Notably, the system effectively distinguished between similar liquids, such as Coke and Pepsi. A few misclassified samples are typically located in adjacent grid spaces, primarily due to neighboring categories’ close feature value similarities. For example, some misclassifications occurred because the liquids possess nearly identical properties, making differentiation more challenging.

Secondly, we designed a series of experiments to thoroughly evaluate LiqState’s ability to detect changes in liquid states. In the primary experiment, we monitored the transition of milk into yogurt, using a pH meter to obtain precise ground truth measurements. Signal data were collected at 30-minute intervals to capture the progression of state changes. In addition to milk, we tested four other liquids: Water, Pepsi, Green Tea, and Honey. To further assess LiqState’s performance, we prepared a diluted honey sample by mixing it with water and a sugar solution by dissolving sugar in water. These liquids were then altered through solute concentration adjustments, allowing us to evaluate LiqState’s capability to detect state changes in solutions with varying compositions. As shown in Tab. IV, we quantified LiqState’s performance using the Root Mean Square Error (RMSE), which measures the deviation between the predicted and actual state changes. The RMSE values for detecting state transitions across these five liquid categories averaged 0.262, demonstrating LiqState’s accuracy and reliability in distinguishing between the initial and altered states of liquids.

Minor Changes in Liquid State: To evaluate LiqState’s performance in detecting minor changes, we introduced a 0.1% syrup solution to five different liquids: water, milk, Pepsi, vinegar, and juice. This small concentration change was designed to assess the system’s sensitivity to subtle variations in the composition of each liquid. As shown in Fig. 13a LiqState demonstrated excellent performance, achieving an average accuracy of 94.5% in detecting minor liquid state changes at a concentration of 0.1%. This level of precision is particularly crucial in applications where even slight changes in liquid state can significantly impact quality. By effectively identifying these subtle liquid states.

Major Changes in Liquid State: We evaluated LiqState’s ability to detect significant liquid state transformations by monitoring key processes affecting physical and chemical properties. The first experiment tracked milk fermentation into yogurt, assessing molecular-level changes. We also examined

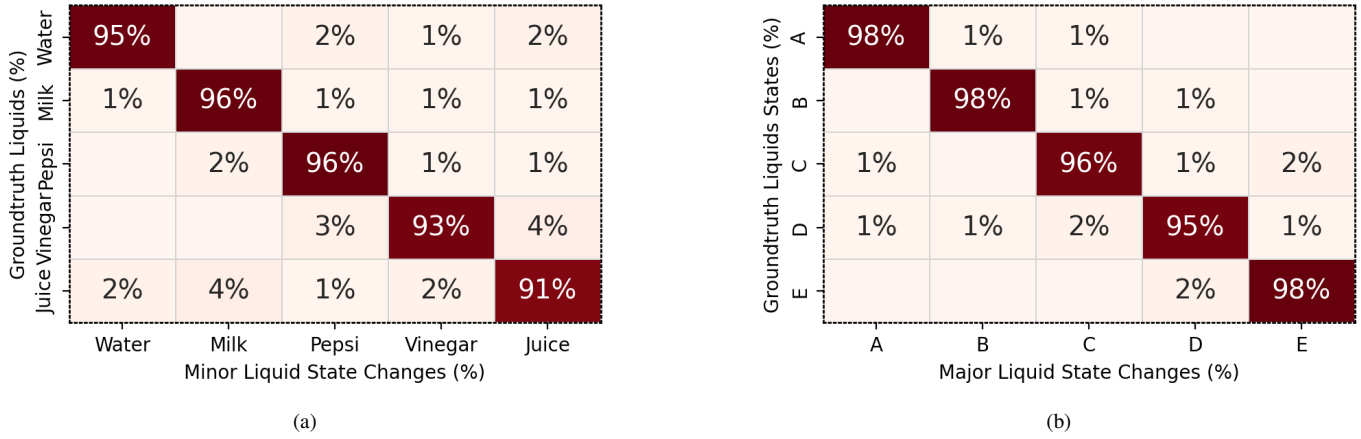


Fig. 13: Performance evaluation of LiqState in identifying minor and major changes in liquids, A, B, C, D, and E represents fermentation, gelling, crystallization, curdling, and solidification.

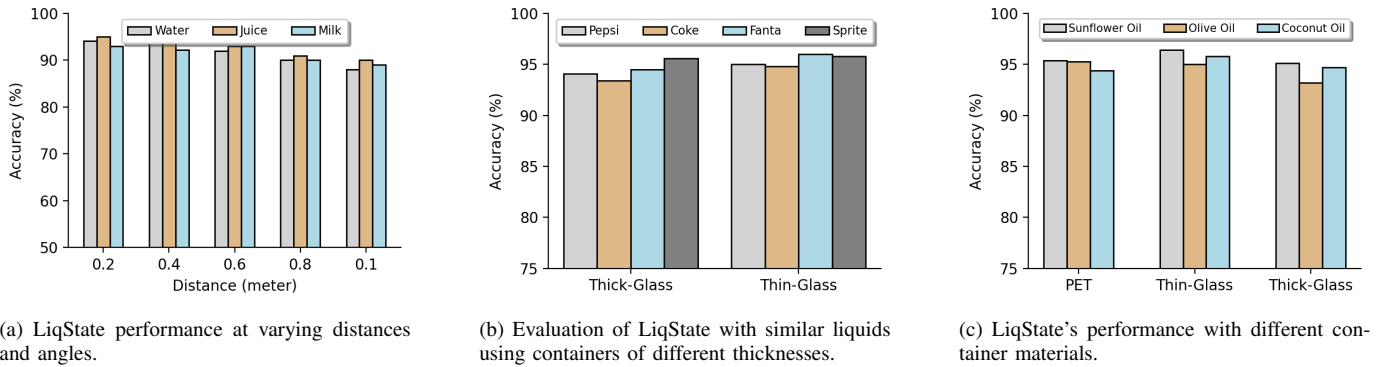


Fig. 14: Performance evaluation of LiqState in detecting liquid states and identifying similar liquids using different container types and at varying distances.

gelling (jelly formation), crystallization (cooling a saturated sugar solution), curdling (adding lemon juice to milk), and solidification (cooling liquid chocolate). These diverse transformations provided a comprehensive assessment of LiqState's accuracy in detecting major state changes.

As shown in Fig. 13b, LiqState achieved 97% accuracy in identifying minor state changes. Its real-time monitoring capabilities make it valuable for food processing, pharmaceuticals, and chemical manufacturing, ensuring precise control over processes like fermentation, crystallization, and solidification, with early detection of spoilage or inconsistencies.

A. Comparison of LiqState with State-of-the-Art Liquid Sensing Methods

We compared LiqState with three advanced liquid identification methods: FG-LiquidID, LiqDetector, and LiqRay+. FG-LiquidID isolates peak zones and calculates the refractive index under controlled distances but lacks robustness when radar-target distance or angle varies. LiqDetector extracts refractive index values using a dual-reflection model but is sensitive to temperature fluctuations, limiting its effectiveness in dynamic environments. LiqRay+ employs a dual-antenna system to classify liquids based on frequency response variation but struggles with fine-grained distinctions under varying angles or

displacements. In contrast, LiqState utilizes a single mmWave receiving antenna to compute VRCP (Viscosity, Refractive Index, Complex Permittivity, and Phase Shift) feature vectors for each sample. The LiqNet model then classifies liquids and monitors state changes with high accuracy. For comparison, we implemented refractive index as a standalone feature alongside the comprehensive VRCP features, adhering to each method's established protocols.

Fine-grained identification Across Varying Distances: The results in Fig. 15a shows that FG-LiquidID, LiqDetector, and LiqRay+ struggle with fine-grained identification under radar-target displacement and angular shifts, achieving 71.3%, 77.2%, and 80.6% accuracy, respectively. In contrast, LiqState maintains over 93.2% accuracy, demonstrating its strong capability for precise liquid identification across varying spatial configurations.

Fine-Grained Identification Using VRCP and Single Features: To assess VRCP against single-feature methods (e.g., refractive index), we evaluated six liquids using 3,000 samples per liquid and 5-fold cross-validation (600 samples per subset). As shown in Fig. 15b, average accuracy across five experiments was 72.7% for FG-LiquidID, 76.5% for LiqDetector, and 82.8% for LiqRay. LiqState outperformed all, achieving 93% accuracy by leveraging VRCP features across the

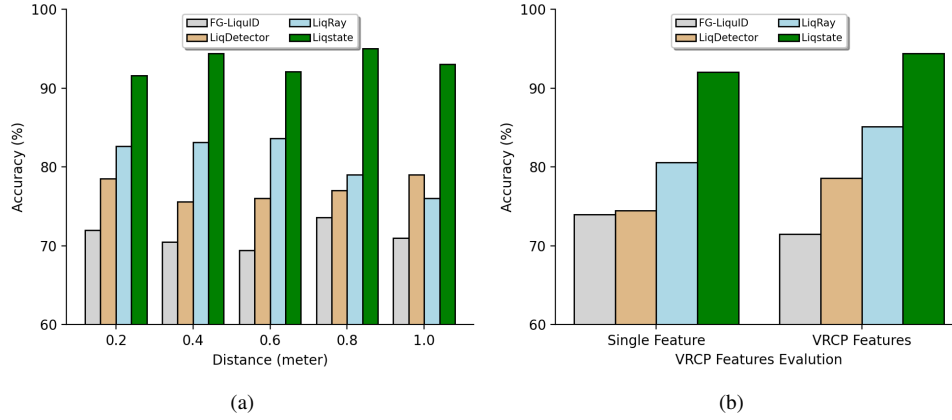


Fig. 15: Comparative analysis of LiqState with existing state-of-the-art liquid sensing methods. (a) Accuracy evaluation of LiqState compared to other models for liquid identification. (b) Performance comparison using VRCP features against single-feature methods for enhanced liquid identification accuracy.

mmWave spectrum for robust fine-grained identification without requiring environmental stability. These results highlight LiqState’s advanced feature extraction, ensuring precise liquid classification and state monitoring across diverse conditions.

B. Micro Benchmark

To thoroughly evaluate the performance of the LiqState system, we conducted a series of micro-benchmark experiments as shown in Fig. 17, designed to assess how various factors impact liquid identification accuracy. Specifically, we explored the influence of radar distance, container material, and liquid temperature on the system’s performance.

Impact of Radar Distance on Liquid Identification: To evaluate the impact of radar-to-container distance on identification accuracy, we conducted experiments with containers placed at five distances: 0.2m, 0.4m, 0.6m, 0.8m, and 1.0m. We collected 180 samples from three liquids at each distance. As shown in Fig. 14a, LiqState achieved 93.4% accuracy for distances up to 0.6m. However, accuracy declined to 89.6% between 0.8m and 1.0m due to increased signal attenuation, reducing feature distinction from environmental noise. Future work could explore higher transmission power radars and alternative mmWave systems to enhance long-distance performance.

Impact of Container Material on Liquid Identification: To assess the impact of container materials on LiqState’s accuracy, we conducted experiments using containers of varying materials and thicknesses. First, we tested its ability to differentiate four similar liquids, Pepsi, Coca-Cola, Sprite, and Fanta inside both thick-glass and thin-glass cylindrical containers. As shown in Fig. 14b, LiqState achieved an average accuracy of 94.9%, effectively distinguishing similar liquids even in reflective environments.

Next, we evaluated its performance in identifying sunflower, coconut, and olive oils in PET, thin glass, and thick glass containers. We collected 540 samples per container type for robust testing. As shown in Fig. 14c, LiqState achieved accuracy rates of 95% for plastic, 95.7% for thin glass, and 94.3% for thick glass. These results confirm that while container material

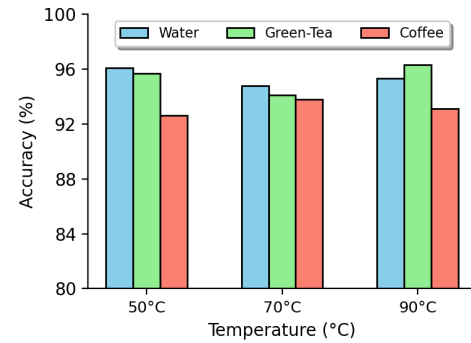


Fig. 16: LiqState performance evaluation at different liquid temperatures

and thickness influence signal behavior, LiqState maintains high accuracy, demonstrating its practical potential for food packaging and oil quality control.

Impact of Liquid Temperature on Identification: In this experiment, we examined the effect of temperature on liquid identification by using drinking water as the solvent and varying sugar concentrations between 0% and 20%, in 1% increments. The data was collected at three distinct water temperatures: 50°C, 70°C, and 90°C, which were selected to assess how temperature fluctuations influence the identification process. A glass container with built-in temperature control, capable of holding 0.5 liters, was used to ensure stable conditions throughout the experiment. For each combination of temperature and sugar concentration, 60 independent measurements were taken, providing a robust data set for analysis. As depicted in Fig. 16, LiqState achieved an average accuracy exceeding 94.6% across all temperatures, demonstrating its reliability in detecting liquid variations regardless of thermal changes.

C. Macro Benchmark

To assess the performance and reliability of LiqState, we carried out a series of practical experiments under different

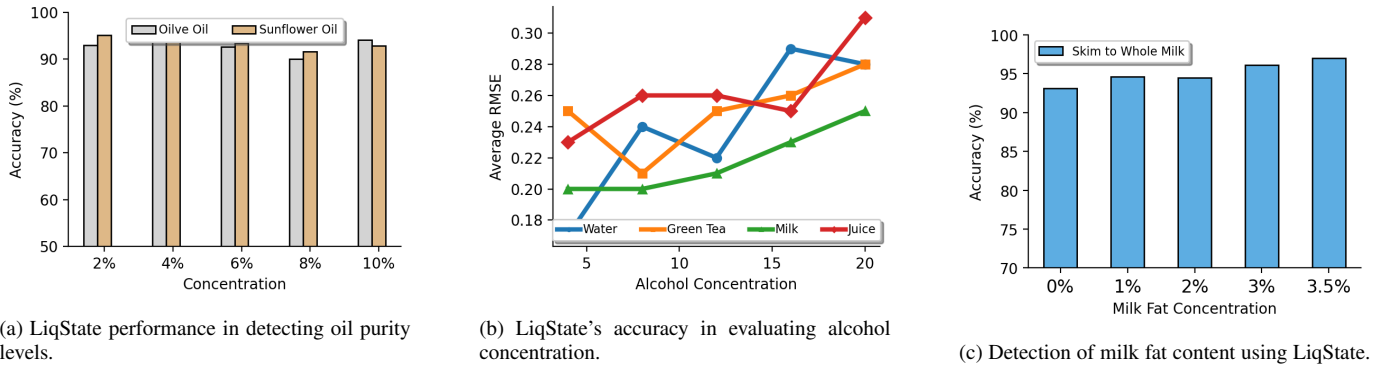


Fig. 17: Performance evaluation of LiqState across various liquid properties, including oil purity, alcohol concentration, and milk fat content detection.

real-world conditions, as presented in Table V. These tests evaluated the system's accuracy in detecting and classifying various liquid properties in practical applications. The results indicate that LiqState's effectiveness in identifying alcohol concentration, oil purity, milk fat content, and coffee strength. Each experiment underscores the practical utility of LiqState in maintaining quality control and ensuring product integrity across diverse use cases.

TABLE V: Macro Benchmark Results in Liquid State Monitoring

Liquids Experiments	RMSE
Alcohol Concentration Detection	0.316
Oil Purity Detection	0.251
Milk Fat Content Detection	0.279
Coffee Strength Detection	0.314
Average RMSE	0.290

Alcohol Concentration Detection: Precise alcohol measurement is essential for beverage quality and regulatory compliance. We tested LiqState's accuracy on liquids such as water, coke, juice, and lemonade, with alcohol concentrations from 4% to 20%. Analyzing properties like viscosity, refractive index, permittivity, and phase shifts, LiqState achieved an RMSE of 0.316 across 100 samples (see Fig. 17b), showcasing its capability for high-precision monitoring in alcohol production industries.

Oil Purity Detection: Oil purity is critical for food safety and consumer trust. We tested LiqState on cooking oil samples adulterated with 5% to 10% sunflower and olive oil. Across the samples (see Fig. 17a), LiqState achieved 93.2% accuracy, demonstrating strong reliability for detecting adulterated oils, crucial for food safety and regulatory compliance.

Milk Fat Content Detection: Fat content is a key quality indicator in milk, impacting nutrition and taste. Using skim (0% fat) and whole milk (3.5% fat) samples, LiqState analyzed viscosity and permittivity. As shown in Fig. 17c, the system achieved 94.8% accuracy in differentiating fat levels, aiding manufacturers in meeting labeling standards and ensuring product consistency.



Fig. 18: LiqState experimental setup for the fermentation of milk into yogurt

D. Case Study

We present two case studies demonstrating the use of LiqState for monitoring liquid state changes: (i) the fermentation of milk into yogurt, and (ii) the ripening of fruit juice at room temperature. These case studies highlight LiqState's effectiveness in tracking real-time liquid transformations, making it valuable for both domestic and industrial applications.

1) Monitoring the Fermentation of Milk into Yogurt: This case study uses LiqState to monitor the fermentation of milk into yogurt, demonstrating its potential for both household and industrial use, where tracking liquid states is essential for quality control. The experiment was conducted over 4 hours at a constant temperature of 42°C in a closed box to optimize fermentation. A testo-206-pH2 meter and mmWave radar were used to measure acidity and physical properties. The milk started at a pH of 6.4 (Fig. 18), which decreased to 4.0 as it turned into yogurt, within the optimal PH range of 4.0 to 4.5 [40]. Data were collected every 30 minutes, with 60 samples per session. The radar tracked viscosity, permittivity, and phase shifts, capturing the milk's transformation. LiqState achieved an RMSE of 0.251, demonstrating its precision in monitoring fermentation. This study showcases LiqState's potential for home yogurt production and industrial scale monitoring, ensuring consistent quality and process optimization.

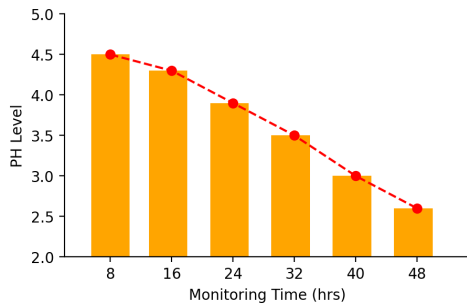


Fig. 19: Orange juice PH-Level decreases with time

E. Monitoring the Ripening Process of Fruit Juice at room temperature

This case study investigates the ripening of orange juice at room temperature, tracking subtle biochemical changes such as pH and flavor during the process. These changes are crucial for flavor and shelf life, and LiqState provides real-time insights into the juice's ripening. The experiment ran for 48 hours at 30°C with freshly squeezed juice stored in sealed containers. The initial pH was 4.5, decreasing to 2.6 by the end, indicating natural ripening (Fig. 19). LiqState monitored the juice properties every 8 hours, with 100 samples per session. The mmWave radar tracked permittivity, phase shift, and viscosity, revealing changes in the juice's composition. Phase shifts correlated with changes in pH, showing LiqState's ability to monitor ripening and fermentation. The LiqNet model was applied to track changes in permittivity, phase shift, and viscosity, with an RMSE of 0.162, indicating high accuracy. The radar data, combined with pH readings, provided a comprehensive view of the ripening process. This study suggests LiqState could be used for quality control in the juice industry, monitoring freshness and avoiding over-ripening. The technology could also apply to other liquid products like smoothies or wines.

VIII. CONCLUSION

This paper introduced a novel mmWave-based approach for liquid identification and state monitoring, leveraging the VRCP feature extraction model, which incorporates viscosity, refractive index, complex permittivity, and phase shift. Using our custom deep learning model, LiqNet, we accurately identified 12 liquids and detected both minor and major state changes. Extensive experiments confirmed high accuracy across real-world scenarios, even under varying conditions. Additionally, two case studies, milk fermentation into yogurt and juice ripening in cold storage—demonstrated LiqState's practical applications for fine-grained liquid monitoring. Its non-invasive, container-independent design ensures broad applicability in industries such as food safety, chemical processing, and healthcare, providing a scalable and reliable solution for liquid identification and monitoring.

REFERENCES

- [1] Y. Yang, Y. Wang, J. Cao, and J. Chen, "Hearliquid: nonintrusive liquid fraud detection using commodity acoustic devices," *IEEE internet of things journal*, vol. 9, no. 15, pp. 13 582–13 597, 2022.
- [2] S. Yue and D. Katabi, "Liquid testing with your smartphone," in *Proceedings of the 17th Annual International Conference on Mobile Systems, Applications, and Services*, 2019, pp. 275–286.
- [3] A. A. Note, "Agilent basics of measuring the dielectric properties of materials," *Agilent literature number*, pp. 1–34, 2006.
- [4] C. Riesch, E. K. Reichel, F. Keplinger, and B. Jakoby, "Characterizing vibrating cantilevers for liquid viscosity and density sensing," *Journal of sensors*, 2008.
- [5] Y. Yang, Y. Wang, J. Cao, and J. Chen, "Hearliquid: nonintrusive liquid fraud detection using commodity acoustic devices," *IEEE internet of things journal*, vol. 9, no. 15, pp. 13 582–13 597, 2022.
- [6] A. Dhekne, M. Gowda, Y. Zhao, H. Hassanieh, and R. R. Choudhury, "Liquid: A wireless liquid identifier," in *Proceedings of the 16th annual international conference on mobile systems, applications, and services*, 2018, pp. 442–454.
- [7] P. Donato, F. Cacciola, P. Q. Tranchida, P. Dugo, and L. Mondello, "Mass spectrometry detection in comprehensive liquid chromatography: basic concepts, instrumental aspects, applications and trends," *Mass spectrometry reviews*, vol. 31, no. 5, pp. 523–559, 2012.
- [8] J. Wang, J. Xiong, X. Chen, H. Jiang, R. K. Balan, and D. Fang, "Tagscan: Simultaneous target imaging and material identification with commodity rfid devices," in *Proceedings of the 23rd Annual International Conference on Mobile Computing and Networking*, 2017, pp. 288–300.
- [9] B. Xie, J. Xiong, X. Chen, E. Chai, L. Li, Z. Tang, and D. Fang, "Tagtag: Material sensing with commodity rfid," in *Proceedings of the 17th conference on embedded networked sensor systems*, 2019, pp. 338–350.
- [10] C. Feng, J. Xiong, L. Chang, J. Wang, X. Chen, D. Fang, and Z. Tang, "Wimi: Target material identification with commodity wi-fi devices," in *2019 IEEE 39th International Conference on Distributed Computing Systems (ICDCS)*. IEEE, 2019, pp. 700–710.
- [11] Y. Liang, A. Zhou, H. Zhang, X. Wen, and H. Ma, "Fg-liquid: A contactless fine-grained liquid identifier by pushing the limits of millimeter-wave sensing," *Proceedings of the ACM on Interactive, Mobile, Wearable and Ubiquitous Technologies*, vol. 5, no. 3, pp. 1–27, 2021.
- [12] Y. Huang, K. Chen, Y. Huang, L. Wang, and K. Wu, "Vi-liquid: unknown liquid identification with your smartphone vibration," in *Proceedings of the 27th Annual International Conference on Mobile Computing and Networking*, 2021, pp. 174–187.
- [13] F. Niaz, J. Zhang, M. Khalid, M. Younas, and A. Niaz, "mmfruit: A contactless and non-destructive approach for fine-grained fruit moisture sensing using millimeter-wave technology," *IEEE Transactions on Mobile Computing*, 2024.
- [14] Z. Wang, Y. Guo, Z. Ren, W. Song, Z. Sun, C. Chen, B. Guo, and Z. Yu, "Liqdetector: Enabling container-independent liquid detection with mmwave signals based on a dual-reflection model," *Proceedings of the ACM on Interactive, Mobile, Wearable and Ubiquitous Technologies*, vol. 7, no. 4, pp. 1–24, 2024.
- [15] F. Shang, P. Yang, Y. Yan, and X.-Y. Li, "Contactless and fine-grained liquid identification utilizing sub-6ghz signals," *IEEE Transactions on Mobile Computing*, 2023.
- [16] —, "Packquid: In-packet liquid identification using rf signals," *Proceedings of the ACM on Interactive, Mobile, Wearable and Ubiquitous Technologies*, vol. 6, no. 4, pp. 1–27, 2023.
- [17] Y. Huang, K. Chen, Y. Huang, L. Wang, and K. Wu, "A portable and convenient system for unknown liquid identification with smartphone vibration," *IEEE Transactions on Mobile Computing*, vol. 22, no. 4, pp. 1894–1911, 2021.
- [18] C. Blakley, J. Carmody, and M. Vestal, "Liquid chromatograph-mass spectrometer for analysis of nonvolatile samples," *Analytical Chemistry*, vol. 52, no. 11, pp. 1636–1641, 1980.
- [19] J. F. Federici, "Review of moisture and liquid detection and mapping using terahertz imaging," *Journal of Infrared, Millimeter, and Terahertz Waves*, vol. 33, pp. 97–126, 2012.
- [20] C. Shi, J. Zhu, M. Xu, X. Wu, and Y. Peng, "An approach of spectra standardization and qualitative identification for biomedical materials based on terahertz spectroscopy," *Scientific Programming*, vol. 2020, no. 1, p. 8841565, 2020.
- [21] T. Rahman, A. T. Adams, P. Schein, A. Jain, D. Erickson, and T. Choudhury, "Nutralizer: A mobile system for characterizing liquid food with photoacoustic effect," in *Proceedings of the 14th ACM Conference on Embedded Network Sensor Systems CD-ROM*, 2016, pp. 123–136.
- [22] Q. Huang, Z. Yang, and Q. Zhang, "Smart-u: smart utensils know what you eat," in *IEEE INFOCOM 2018-IEEE Conference on Computer Communications*. IEEE, 2018, pp. 1439–1447.

- [23] H. Matsui, T. Hashizume, and K. Yatani, "AI-light: An alcohol-sensing smart ice cube," *Proceedings of the ACM on interactive, mobile, wearable and ubiquitous technologies*, vol. 2, no. 3, pp. 1–20, 2018.
- [24] A. Zhou, S. Yang, Y. Yang, Y. Fan, and H. Ma, "Autonomous environment mapping using commodity millimeter-wave network device," in *IEEE INFOCOM 2019-IEEE Conference on Computer Communications*. IEEE, 2019, pp. 1126–1134.
- [25] F. Adib, Z. Kabelac, D. Katabi, and R. C. Miller, "3d tracking via body radio reflections," in *11th USENIX Symposium on Networked Systems Design and Implementation (NSDI 14)*, 2014, pp. 317–329.
- [26] B. Zhou, Q. Chen, and P. Xiao, "The error propagation analysis of the received signal strength-based simultaneous localization and tracking in wireless sensor networks," *IEEE Transactions on Information Theory*, vol. 63, no. 6, pp. 3983–4007, 2017.
- [27] F. Niaz, J. Zhang, Y. Zheng, M. Khalid, and A. Niaz, "mm-cur: A novel ubiquitous, contact-free, and location-aware counterfeit currency detection in bundles using millimeter-wave sensor," *ACM Transactions on Sensor Networks*, 2024.
- [28] F. Niaz, J. Zhang, M. Khalid, K. N. Qureshi, Y. Zheng, M. Younas, and N. Imran, "Ai enabled: a novel iot-based fake currency detection using millimeter wave (mmwave) sensor," *Computing*, vol. 106, no. 8, pp. 2851–2873, 2024.
- [29] Z. Yang, P. H. Pathak, Y. Zeng, X. Liran, and P. Mohapatra, "Monitoring vital signs using millimeter wave," in *Proceedings of the 17th ACM international symposium on mobile ad hoc networking and computing*, 2016, pp. 211–220.
- [30] F. Wang, F. Zhang, C. Wu, B. Wang, and K. R. Liu, "Vimo: Vital sign monitoring using commodity millimeter wave radio," in *ICASSP 2020-2020 IEEE international conference on acoustics, speech and signal processing (ICASSP)*. IEEE, 2020, pp. 8304–8308.
- [31] S. Wang, J. Song, J. Lien, I. Poupyrev, and O. Hilliges, "Interacting with soli: Exploring fine-grained dynamic gesture recognition in the radio-frequency spectrum," in *Proceedings of the 29th annual symposium on user interface software and technology*, 2016, pp. 851–860.
- [32] I. W. Selesnick and C. S. Burrus, "Generalized digital butterworth filter design," *IEEE Transactions on signal processing*, vol. 46, no. 6, pp. 1688–1694, 1998.
- [33] S. Jurdak, M.-S. Alouini, T. Kiuru, M. Metso, and S. Ahmed, "Compact mmwave fmcw radar: Implementation and performance analysis," *IEEE Aerospace and Electronic Systems Magazine*, vol. 34, no. 2, pp. 36–44, 2019.
- [34] J. A. Shaw, "Radiometry and the riis transmission equation," *American journal of physics*, vol. 81, no. 1, pp. 33–37, 2013.
- [35] A. P. Gregory and R. Clarke, "Tables of the complex permittivity of dielectric reference liquids at frequencies up to 5 ghz." 2012.
- [36] C. F. Bohren and D. R. Huffman, *Absorption and scattering of light by small particles*. John Wiley & Sons, 2008.
- [37] W. Ellison, "Permittivity of pure water, at standard atmospheric pressure, over the frequency range–25thz and the temperature range–100 c," *Journal of physical and chemical reference data*, vol. 36, no. 1, pp. 1–18, 2007.
- [38] M. Schwartz, *Principles of electrodynamics*. Courier Corporation, 2012.
- [39] Texas Instruments, "IWR1443 Single-Chip 76-GHz to 81-GHz mmWave Sensor," 2025, accessed: 2025-02-07. [Online]. Available: <https://www.ti.com/lit/ds/symlink/iwr1443.pdf>
- [40] S.-S. Kang, M. K. Kim, and Y.-J. Kim, "Comprehensive evaluation of microbiological and physicochemical properties of commercial drinking yogurts in korea," *Food science of animal resources*, vol. 39, no. 5, p. 820, 2019.



Fahim Niaz is currently a Ph.D. scholar at Wuhan University, China, and received his M.S. in Computer Science from Bahria University, Islamabad, Pakistan, in 2018. From 2017 to 2022, he served as a Lecturer at Higher Education Khyber-Pakhtunkhwa. His research interests include the Internet of Things (IoT), Wireless Sensor Networks, and Millimeter-Wave Radars. Fahim also works as an AI expert at Wuhan University's Institute of Artificial Intelligence, specializing in transfer learning and advanced deep learning models.



Jian Zhang received the B.S., M.S., and Ph.D. degrees in computer architecture from Wuhan University, Wuhan, China, in 1998, 2001, and 2006, respectively. He is currently a professor in the School of Computer Science at Wuhan University. His research interests include Cloud Computing, the Internet of Things (IoT), and Big Data.



Muhammad Khalid is currently a Lecturer (Assistant Professor) in Computer Science at the School of Computer Science, University of Hull. Previously, he was a Post-Doctoral Research Fellow at the University of Lincoln, where he focused on ensuring robot autonomy with respect to safety considerations. He completed his Ph.D. in 2020 at Northumbria University, specializing in autonomous parking in intelligent smart cities.



Muhammad Younas received his Master's degree in Software Engineering from Northeastern University, China, in 2022. He is currently pursuing a Ph.D. at the School of Computer Science, Wuhan University, China. His research interests include the Internet of Things (IoT), Wireless Sensor Networks, Millimeter-Wave Radars, Artificial Intelligence, Machine Learning, and Blockchain.



Abdul Majid received his Master's degree in Computer Science and Technology from Central China Normal University, China, in 2019. He is currently pursuing a Ph.D. at the School of Computer Science, Wuhan University, China. His research interests include the Computer Vision, Artificial Intelligence, Machine Learning, and Deep Learning.